Understanding the Defect Formation of Thin Ply Composites During Automated Fiber Placement

Von Clyde Jamora
Old Dominion University
Director: Dr. Oleksandr Kravchenko

ABSTRACT

Automated fiber placement is a high throughput manufacturing process that allows for the rapid fabrication of complex composite structures. However, this processing method typically results in irregular morphology due to non-conventional layup designs due to defects. To understand the effects of the manufacturing phenomena a multi-physics model needs to be established to observe the effects of embedded defects on the final morphology of the composite. A model is made through finite element analysis which simulates the compaction through a subroutine. The subroutine uses a visco-hyperelastic consisting of an elastic and viscous component. While the elastic component uses established hyperelastic equations, the viscous component uses a novel tensorial viscosity approach and multiplicative phenomenological components. A finite element models were made: a single ply with varying widths, and a gap embedded model. Experimental composites were made to validate the finite element models. The single ply model shows good correlation with experimental results and the gap model is shown to properly simulate the complex morphology. However, more physics need to be established in the model for more realistic results.

INTRODUCTION

Novel composite manufacturing processes offer greater control over tailored fiber orientation. An application of such enabling technology is based on introducing continuous fiber either through fused filament additive manufacturing [1]. These manufacturing methods [1], [2] can be used to rapidly produce composites with greater flexibility by optimizing manufacturing parameters based on loading conditions through a tailored stiffness structure. The central focus of the work is on automated fiber placement (AFP), which is a state-of-the-art high throughput method that allows for the fabrication of advanced composites structures [3]. AFP systems can lay down tailored tow paths to create variable fiber orientations and thickness [4]. The AFP working principle is schematically shown in figure 1(a). Unlike other conventional manufacturing methods, AFP allows for the rapid and efficient manufacturing of complex structures [5]–[7] such as deployable space structure and structural elements in launch vehicles. However, these novel processing methods for advanced polymeric composites typically result in an irregular morphology during fabrication, the development of which can be explained by the manufacturing process [8]. More specifically, AFP made composites exhibit morphological variability on the micro-scale, including ply thickness variation, ply waviness, and large pockets due to the deposition and consolidation process [8]. These manufacturing defects influence the resulting mechanical properties, therefore a relationship between the material's synthesis and performance needs to be established. Technology such as AFP expands the design space but needs to be further studied to increase its reliability. Uncertainties in manufacturing hinder the process and must be analyzed to enhance the reproducibility of AFP made composite structures.

Manufacturing defects are created during early stages of curing and compaction before resin gelation and significantly affect the mechanical properties of the composites [9] with a major part of the deformation attributed to the cooling process [10]. Formation of morphological micro- and meso- structural features can be traced to large, non-linear deformations of the fiber preform caused by inherent material phenomena and compaction of non-conventional layup designs that cause tow gaps and overlaps (Fig. 1(b)). Since AFP produces a very large combination of various manufacturing imperfections or defects, to utilize this technology to its full capability requires a simulation driven approach to predict the defect morphology using a process modeling framework. Much of the defects can be traced from the manufacturing causing the material orientation to deviate during deposition and compaction [11]. To fully understand the interactions between the material properties and its failure modes, which form on different length scales, the complex morphology must be represented in a physically meaningful way. This approach will enable the understanding of defect feature formation due to manufacturing induced defects through the prism of the complex morphology (fig. 1(c)).

METHODOLOGY

To fully understand the manufacturing phenomena of AFP made composites, the model needs an interconnected physics model outlined in in figure 2. A temperature boundary condition was used to describe the temperature for the heat transfer model. The degree of cure was calculated using autocatalytic kinetics

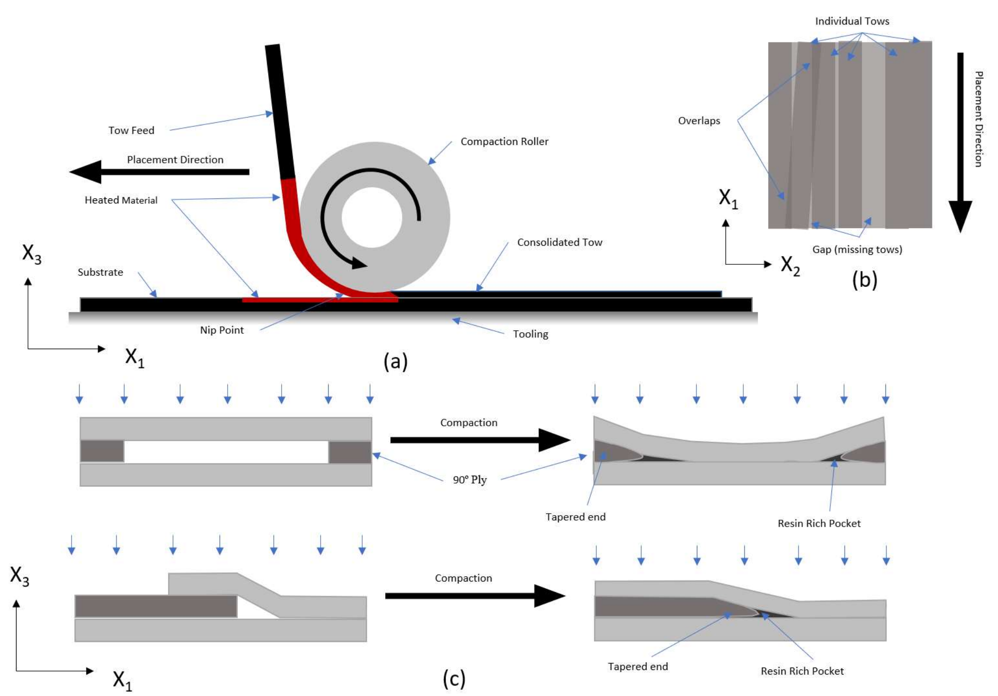

Figure 1. (a) The working principle of an AFP process; (b) Schematic of gaps and overlaps within a ply; (c) Consolidation process at gap and overlap locations.

model [12]. The development of the resin viscosity is derived as a relationship of the degree of cure, and temperature depicted in equation 2 [13]. The constants were derived from literature for 8552 resin[13]].

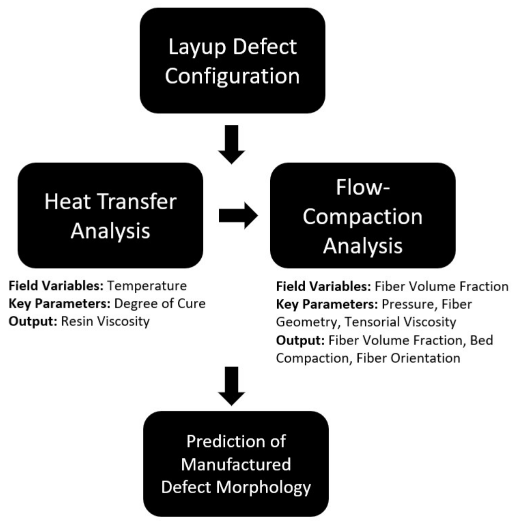

Figure 2. Coupled compaction and heat transfer analysis for predicting defects on AFP manufactured composites

Visco-Hyperelastic Model

A novel approach to modeling the consolidation of uncured composites was implemented based on hyper visco-elastic constitutive model using explicit finite element analysis. The compaction modelling consists of two parts: an elastic model and a viscous model (Fig. 2) [14]. The elastic model is obtained from established transversely isotropic hyperelastic constitutive equations applied to composites [15], [16]. The elastic part of the model uses the deformation gradient to calculate the Cauchy-green deformation tensor, C an create a constitutive equation based on the Helmholtz free energy function, psi.

The liner and anisotropic hyperelastic equation can then be established as an equation through invariants of C. The Piola-Kirchhoff stress tensor is then solved for and used to derive the Cauchy stress tensor by pushed forward operation. Cauchy stress is used directly in the FEA.

Viscous Model

The viscous term consists of multiplicative decomposition of strain and strain rate dependent terms for the apparent viscosity [17]. The approach was based on the previous process modeling work where the viscosity term is divided into three components [14], [18]. One key difference between the existing methods is that for the rate term, a tensorial approach was used due account for the anisotropy of the fiber reinforced composite where the viscous terms are a function of the fiber volume matrix. Where the matrix fluid follows a simple power-law [19]. The apparent tensorial viscosity is a function of the strain rate, fiber volume fraction and the power-law exponent, m The components, multiplied with the strain rate, can then be derived as:

$$\sigma_{11} = 2^{-m\bar{f}} \left[\frac{\sqrt{\bar{f}}}{1-\sqrt{\bar{f}}}\right]^{m} \left(\frac{L}{D}\right)^{m+1} \dot{\epsilon}_{11}{}^{m} \quad (1)$$

$$\sigma_{22} = 2^{m+1} \left[1-\sqrt{\bar{f}}\right]^{-m} \dot{\epsilon}_{22}{}^{m} \quad (2)$$

$$\sigma_{33} = 2^{m+1} \left[1-\sqrt{\bar{f}}\right]^{-m} \dot{\epsilon}_{33}{}^{m} \quad (3)$$

$$\sigma_{23} = \left[1-\sqrt{\bar{f}}\right]^{-m} \dot{\gamma}_{23}{}^{m} \quad (4)$$

$$\sigma_{12} = 2^{-m} \left[\frac{1-\sqrt{\bar{f}}}{1-\sqrt{\bar{f}}}\right]^{m} \dot{\gamma}_{12}{}^{m} \quad (5)$$

where the $\bar{f}$ is the ratio of the fiber volume fraction and the maximum packing fraction based on the geometry. L and D are the fiber length and the fiber diameter respectively and for the FEA model, L is simply the length of the ply. These tensorial viscosities make up the rate term in the overall viscous component calculation.

The viscous ply and micro terms are described using the phenomenological parameters, namely component that govern the apparent viscosity and flow mode on a microscopic scale and the macroscopic ply scale [20]. Squeezing flow occurs when the material is incompressible, and the transverse direction of the ply is proportional to the compaction direction [21].

The ply term depends on an analytical solution based on the geometry and the surface conditions of the ply. No-slip is assumed for the surfaces which was derived by rogers [21]. The ply term is then rearranged by Belnoue [14] to be:

$$\eta_{ply} = 2\left(\frac{w_0}{h_0}\right)^2 e^{-4\varepsilon} \tag{6}$$

Where w_0 is the width of the ply, and h_0, is the height of the ply. The micro term depends on phenomenological parameters that were experimentally determined which was adopted from the research done by Nixon-Pearson et al [20].

$$\eta_{micro} = 2\sqrt{\chi_l}e^{\varepsilon}k\left(\left(\frac{k}{\sqrt{\chi_f}e^{\varepsilon} - k}\right)^2 + 3\right) \tag{7}$$

Where k is a stepwise function of the temperature, χ_l, is the aspect ratio during locking and χ_f, is the final aspect ratio.

FINITE ELEMENT ANALYSIS

A coupled heat transfer and hyper-viscoelastic constitutive model was developed to simulate the highly non-linear material behavior and the large deformations in the defect regions of the fiber tows during compaction. The computational scheme used an explicit scheme in the commercially available finite element analysis software, Abaqus Unified FEA (Dassualt Systemes, Vélizy-Villacoublay, France) with custom-made subroutines.

This work used solution dependent variables, such as the degree of cure, while tracking the fiber orientation throughout the process. The compaction, the visco-hyperelastic model was incorporated through a VUMAT subroutine. VUFIELD was used to supply the material's fiber direction as a vector in global coordinates. The overall goal of the FEA model is to characterize the local morphology variations. The material used in the study is Hexcel IM7/8552 with low tack behavior where the material properties were derived from literature [12]–[14]. The models consisted of C3D8T elements, varying between 168 – 462 nodes depending on width, and used one element through the thickness to simulate a ply.

The conducted test was to simulate a compaction of single ply composites with varying widths. A modeled sample with dimensions of a 50.25x6.46x0.14 mm sample is shown in figure 3(a). A pressure of 0.551 MPa (80 psi) was applied to the top of the material and a heat was delivered through a single hold cure cycle as shown in fig. 4. Six models were simulated, which varied the thickness and the widths of the composite ply. The length is a constant 50.25 mm (2 in.), and the thickness is 0.1397 mm. The width was varied as one ply (6.46 mm), two plies (13.15 mm), and four plies (25.61 mm) laid side by side. The ply is constrained in the through thickness direction at the bottom ply and density of the material is 1590 kg/m^3. However,

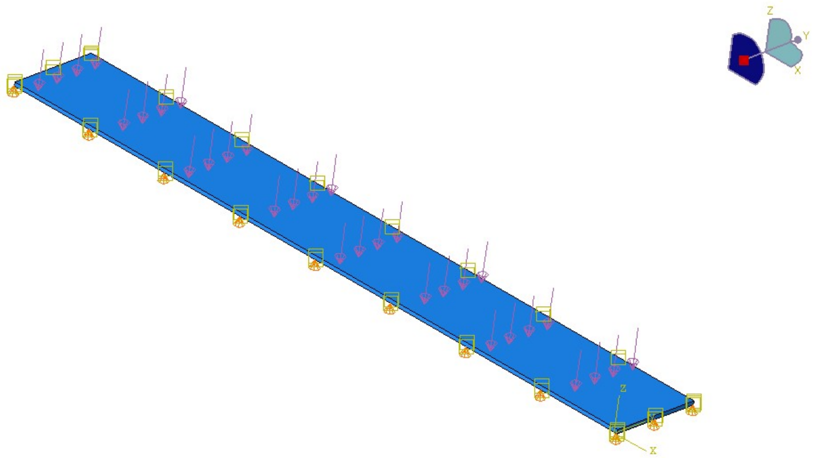

(a)

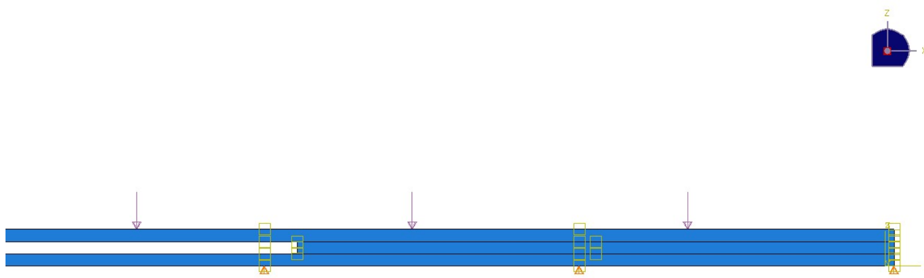

(b)

Figure 3. (a) A typical model of Single ply (b) Half the model of embedded gap model which shows the embedded gap between two 90º plies.

for model stability and increase the processing time, the density of the material was increased.

To test the model further, an embedded defect model was tested with the same properties as the single ply test. The stacking sequence is [0/90/0], as shown in fig 3(b). where a gap is placed in the center 90º ply between two 0º plies. The 0º ply is 25.15x12.65x0.14 mm, the 90º ply is 6.51x12.65x0.14 mm, and gap in between is 12.13x12.65x0.14 mm. The model was subjected under the same pressure conditions and cure cycle. Interactions between the plies are assumed to be no-slip conditions. Boundary conditions restrict vertical degree of freedom to simulate the tooling.

EXPERIMENTAL

As a metric to test the FEA model, the same conditions were applied were applied to composite samples. For the experimental data, the composite was interrupted at the first hold of the manufacture's prescribed cure cycle [22]. Heat was ramped to 110 Cº and interrupted at one hour. The composite was compressed using a heat press that applied the 80 psi of pressure. The change in thickness and width were then measured and averaged after the end of the process. To compare the results of the embedded gap, a microscope was used to observe the amount of deformation around the gap region and compare the experimental results with modeling prediction. A Leica DM6 upright microscope was used to determine the effects of the compaction on the embedded gap.

RESULTS

As expected, the thickness decreases while the width increases for the compaction analysis. The strain of the compaction model shows non-linear behavior for the compaction of the composite which is typical of a visco-hyperelastic curve (fig. 5). Results also show that an increasing number of tows makes the structure stiffer thus decreasing the strain of the thickness.

The experimental data for the composite plies exhibit some a large scatter for the results. However, the comparison between certain experimental data and the numerical simulation of the composite ply shows that the data is well correlated, especially in the single ply thickness results. Both the experimental and numerical data shows that a large drop in strain is present when another ply is added to the width and seems to be plateauing for the strain with further increasing width (Fig. 6).

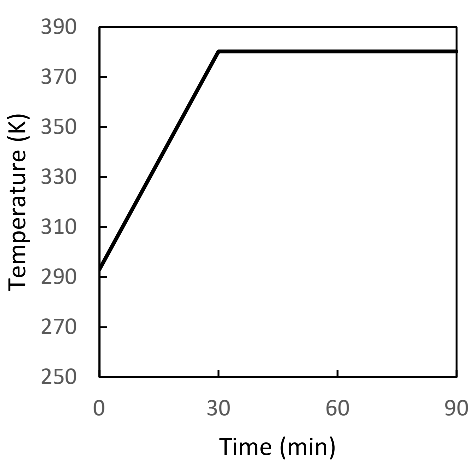

Figure 4. The applied temperature for the single hold

Gap Model

The area of interest for the gap model is at the edge of the 90º ply where both the 0º and 90º ply experiences complex morphology shown in figure 7(a). Due to the non-linear behavior, the logarithmic strain is the metric recorded at 30 minutes 7(b)-7(c) and at one hour 7(d)-7(e) into the hold stage. At 30 minutes, transverse flow has occurred at the 90º degree ply with flow towards the gap (fig 7(b)). The 0º also experiences transverse elongation as the material at the gap is compressed. At one hour, the transverse flow is apparent in both the 0º and 90º. Figure 7(b) and figure 7(d) were recorded at the viewpoint and depicts the 90º ply moving away from the gap due to a substantial elongation in the 0º plies. With the compression of the material, the 0º has expectedly sank into the gap after 30 minutes into the hold stage. However, most of the compressive strain is shown to be in the middle 90 º ply. At one hour, the same trends continue with a significant compression in the at the edge of the 90º ply. Furthermore, the 0º have also experienced further compression which contributes to the elongation at the transverse direction.

In figure 8 the experimental laminate shows that 90º ply is pointing towards the out-of-plane or Y-direction direction which protrudes beyond the 0º for a good visual. The transverse or X-direction is the fiber direction for the 0º ply and the through thickness direction is labeled at the Z-direction. The experimental laminate shows the same sinking 0º degree ply at the gap. The 90º exhibit both transverse and out-of-plane bleeding. Bleeding flow can also be observed in several locations of 0º. Very similar to the FEA model, the

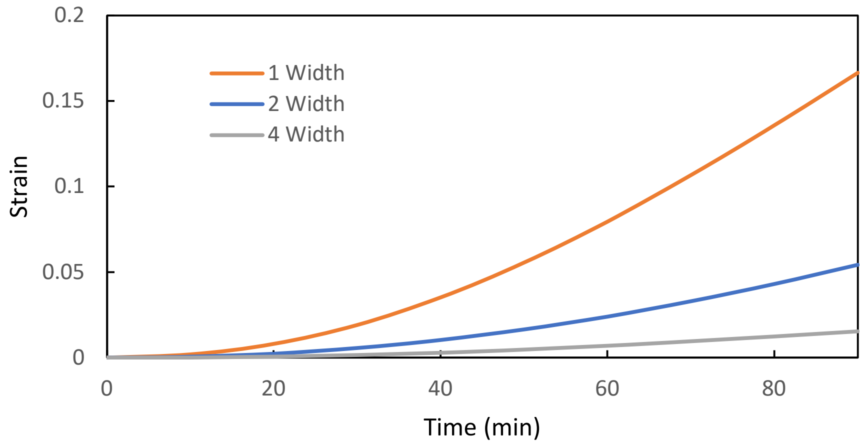

Figure 5. Strain of the composite thickness of the unidirectional models

complex morphology of the process shows a void forming at the edge of the 90º ply where a resin rich region could potentially be created further into the cure cycle. As a metric to compare, the angle of between the two 0º plies was measured. The angle formed by FEA model at the sunken 0º at 30 minutes is 5.37º (fig. 7(c)) and after 4.11º at one hour (fig 7(e)). Compared to the experimental results, the gap shows an angle of 6.47 degrees (fig. 8). The difference in angle and the presence of bleeding shows that not all the compaction phenomena is fully simulated, and further results are needed to truly model an embedded gap.

CONCLUSION

A model was made to simulate the manufacturing of an AFP made composite. The degree of cure, viscosity, and the fiber bed compaction was properly simulated as evident from the unidirectional models. The modeling analysis of the unidirectional models show that there is not a noticeable effect in terms of sizing effect. This show that further work needs to be done for the geometrically dependent term of the viscous components of the compaction model. There is much more work to be done to fully simulate the sizing effects of thin-ply

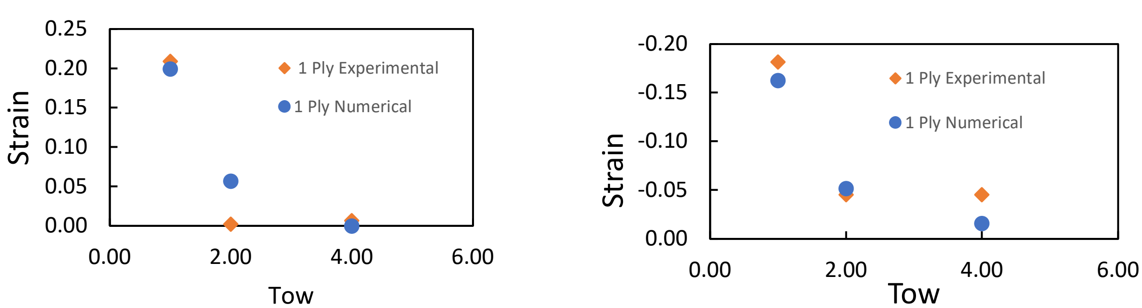

(a) (b)

Figure. 6 (a) Strain for the width for 1 and 2 Ply for Experimental data and Theoretical data from the FEA simulation (b) The strain of thickness for 1 and 2 Ply for Experimental data and Theoretical data from the FEA simulation

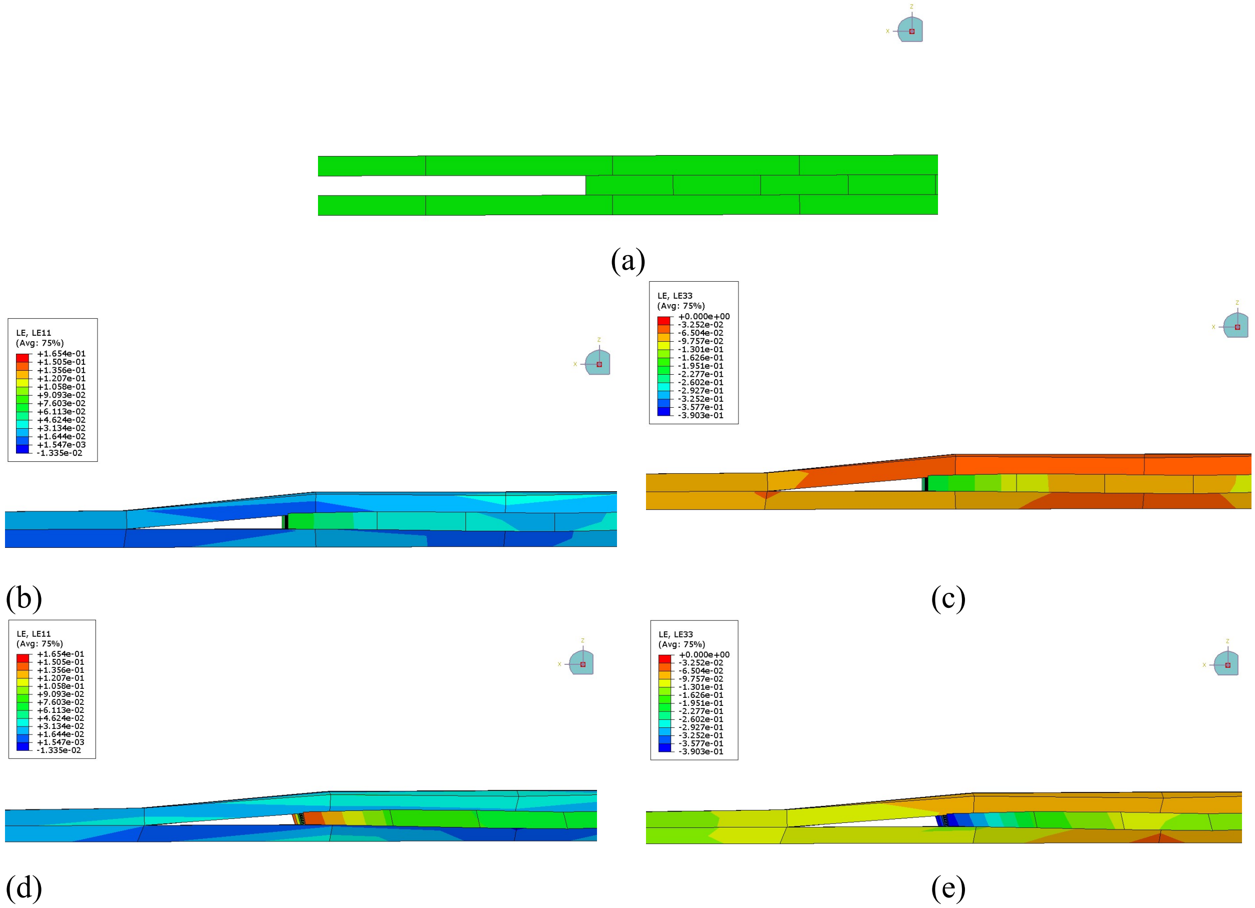

Figure. 7 (a) The undeformed configuration of the gap embedded model taken at the same viewport as the other images (b) The transverse logarithmic strain 30 Minutes into the hold stage (c) The through thickness logarithmic strain 30 minutes into the hold stage. (d) The transverse logarithmic strain 1 hour into the hold stage (e) The through thickness logarithmic strain 1 hour into the hold stage

composites. The model was demonstrated to simulate the compaction a unidirectional composite and multidirectional laminate with the gap model. The preliminary modeling and experimental results show good correlation; however, more experimental work is needed for validation of the numerical model. The experimental composite shows some physical phenomena that is not currently modeled, such as the bleeding flow found throughout the composite. The angle metric also indicates that some physics may be further needed for a mor realistic result.

FUTURE WORK

Much of the physics have been simulated in the model. However, there are more methods that can be integrated for a more realistic model. This includes a locking mechanism that changes the resin flow mode from squeezing to bleeding flow. A metric is needed to be determined to check for locking at a material point. Furthermore, the interactions between the plies should also be considered along with running models with thicker composites that are subject to exothermic heating conditions from the curing resin. The current model assumes a constant fiber volume fraction; however, the future models will incorporate a variable fiber volume fraction based on the current state of the composite material and further analysis on the changes in material orientation needs to be observed. Along with the gap, an overlap model will also be made to study the effects of all types of defects. Furthermore, the microstructure variability will be analyzed to determine validate the numerical results of the compaction mode.

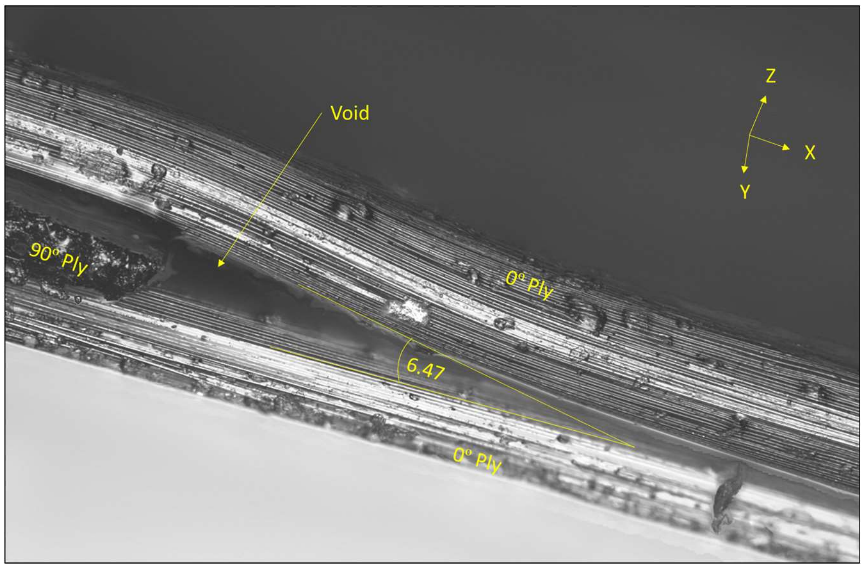

Figure 8. A micrograph of a laminate with an embedded gap. The 0 º ply is shown to sink and form a void at the edge of the 90º ply.

REFERENCES

[1] D. H.-J. A. Lukaszewicz, C. Ward, and K. D. Potter, "The engineering aspects of automated prepreg layup: History, present and future," *Compos. Part B Eng.*, vol. 43, no. 3, Art. no. 3, Apr. 2012, doi: 10.1016/j.compositesb.2011.12.003.

[2] K. S. Madhok, "Comparative characterization of Out-of-Autoclave Materials made by Automated Fiber Placement and Hand-Lay-Up Processes," masters, Concordia University, 2013.

[3] K. C. Wu, "Design and analysis of tow-steered composite shells using fiber placement," 2008.

[4] K. Wu *et al.*, "Design and Manufacturing of Tow-Steered Composite Shells Using Fiber Placement," in *50th AIAA/ASME/ASCE/AHS/ASC Structures, Structural Dynamics, and Materials Conference*, 0 vols., American Institute of Aeronautics and Astronautics, 2009.

[5] M. Bannister, "Challenges for composites into the next millennium — a reinforcement perspective," *Compos. Part Appl. Sci. Manuf.*, vol. 32, no. 7, Art. no. 7, Jul. 2001, doi: 10.1016/S1359-835X(01)00008-2.

[6] H. B. Olsen and J. J. Craig, "Automated composite tape lay-up using robotic devices," in *[1993] Proceedings IEEE International Conference on Robotics and Automation*, May 1993, pp. 291–297 vol.3, doi: 10.1109/ROBOT.1993.292190.

[7] M. N. Grimshaw, C. G. Grant, and J. M. L. Diaz, “Advanced technology tape laying for affordable manufacturing of large composite structures,” *Int. SAMPE Symp. Exhib. Proc.*, vol. 46, pp. 2484–2494, Jan. 2001.
[8] K. Croft, L. Lessard, D. Pasini, M. Hojjati, J. Chen, and A. Yousefpour, “Experimental study of the effect of automated fiber placement induced defects on performance of composite laminates,” *Compos. Part Appl. Sci. Manuf.*, vol. 42, no. 5, Art. no. 5, May 2011, doi: 10.1016/j.compositesa.2011.01.007.
[9] X. Li, S. R. Hallett, and M. R. Wisnom, “Modelling the effect of gaps and overlaps in automated fibre placement (AFP)-manufactured laminates,” *Sci. Eng. Compos. Mater.*, vol. 22, no. 2, pp. 115–129, 2015, doi: 10.1515/secm-2013-0322.
[10] R. J. Young, R. J. Day, M. Zakikhani, and I. M. Robinson, “Fibre deformation and residual thermal stresses in carbon fibre reinforced PEEK,” *Compos. Sci. Technol.*, vol. 34, no. 3, Art. no. 3, Jan. 1989, doi: 10.1016/0266-3538(89)90031-6.
[11] F. Heinecke and C. Willberg, “Manufacturing-Induced Imperfections in Composite Parts Manufactured via Automated Fiber Placement,” *J. Compos. Sci.*, vol. 3, Jun. 2019, doi: 10.3390/jcs3020056.
[12] P. Hubert, A. Johnston, A. Poursartip, and K. Nelson, “Cure kinetics and viscosity models for Hexcel 8552 epoxy resin,” *Int SAMPE Symp Exhib.*, vol. 46, pp. 2341–2354, Jan. 2001.
[13] S. J. Ng, R. Boswell, S. J. Claus, F. Arnold, and A. Vizzini, “Degree of Cure, Heat of Reaction, and Viscosity of 8552 and 977-3 HM Epoxy Resin,” NAVAL AIR WARFARE CENTER AIRCRAFT DIV PATUXENT RIVER MD, Mar. 2000. Accessed: Mar. 16, 2021. [Online]. Available: https://apps.dtic.mil/sti/citations/ADA377439.
[14] J. P.-H. Belnoue, O. J. Nixon-Pearson, D. Ivanov, and S. R. Hallett, “A novel hyper-viscoelastic model for consolidation of toughened prepregs under processing conditions,” *Mech. Mater.*, vol. 97, pp. 118–134, Jun. 2016, doi: 10.1016/j.mechmat.2016.02.019.
[15] G. Limbert and J. Middleton, “A transversely isotropic viscohyperelastic material: Application to the modeling of biological soft connective tissues,” *Int. J. Solids Struct.*, vol. 41, no. 15, Art. no. 15, Jul. 2004, doi: 10.1016/j.ijsolstr.2004.02.057.
[16] J. Bonet and A. J. Burton, “A simple orthotropic, transversely isotropic hyperelastic constitutive equation for large strain computations,” *Comput. Methods Appl. Mech. Eng.*, vol. 162, no. 1, Art. no. 1, Aug. 1998, doi: 10.1016/S0045-7825(97)00339-3.
[17] P. A. Kelly, “A viscoelastic model for the compaction of fibrous materials,” *J. Text. Inst.*, vol. 102, no. 8, pp. 689–699, Aug. 2011, doi: 10.1080/00405000.2010.515103.
[18] E. L. Wang and T. G. Gutowski, “Laps and gaps in thermoplastic composites processing,” *Compos. Manuf.*, vol. 2, no. 2, pp. 69–78, Jan. 1991, doi: 10.1016/0956-7143(91)90182-G.
[19] R. B. Pipes, “Anisotropic Viscosities of an Oriented Fiber Composite with a Power-Law Matrix,” *J. Compos. Mater.*, vol. 26, no. 10, pp. 1536–1552, Oct. 1992, doi: 10.1177/002199839202601009.
[20] O. Nixon-Pearson, J. Belnoue, D. Ivanov, and S. Hallett, “THE COMPACTION BEHAVIOUR OF UN-CURED PREPREGS,” Jul. 2015.
[21] T. G. Rogers, “Squeezing flow of fibre-reinforced viscous fluids,” *J. Eng. Math.*, vol. 23, no. 1, pp. 81–89, Mar. 1989, doi: 10.1007/BF00058434.
[22] “HexPly® 8551-7 Epoxy Matrix Product Data Sheet.” HEXCEL®, Accessed: Mar. 31, 2021. [Online]. Available: https://www.hexcel.com/user_area/content_media/raw/HexPly_85517_us_DataSheet.pdf.